Heliyon 9 (2023) e20628

Contents lists available at ScienceDirect

Heliyon

journal homepage: www.cell.com/heliyon

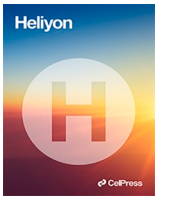

The firing temperatures of burnt clay from the Chinese neolithic cultural relics and its paleoenvironmental imprints

Guishan Chen [a,b], Guanhua Li [a,b,*], Miaomiao Liu [a,b], Wei Ge [c,**], Guibin Wu [d], Changfa Zhan [b]

[a] Guangdong Provincial Key Laboratory of Marine Disaster Prediction and Prevention, College of Science, Shantou University, Shantou, 515063, Guangdong, China
[b] Southern Marine Science and Engineering Guangdong Laboratory (Zhuhai), Zhuhai, 519000, Guangdong, China
[c] Laboratory of Archaeometry, School of History and Cultural Heritage, Xiamen University, Xiamen, 361005, Fujian, China
[d] Pucheng Museum, Nanping, 354200, Fujian, China

ARTICLE INFO

Keywords:
Magnetic properties
Firing temperatures
Paleoenvironment
Neolithic burnt clay
The eurasia

ABSTRACT

The impact of human-induced fires on the surrounding environment has been particularly significant during the Anthropocene epoch. Neolithic burnt clay, which is widely distributed in the archaeological relics of ancient civilizations across the Eurasian continent, provides pivotal information about the ancient firing stories. However, understanding of the paleoenvironmental imprints of fire in burnt clay has been largely limited by the lack of sufficient analytical data on comprehensive knowledge of ancient firing conditions. In this study, a detailed magnetic analysis was conducted on burnt clay materials from a Neolithic site in Fujian, southeastern China, which presented a burnt clay-based record of the Neolithic firing temperature in relation to paleoenvironmental conditions. Based on magnetic analysis, the ancient firing temperature was determined to be approximately 620 °C, which is comparable with other records from Eurasian Neolithic sites. Frequency-dependent magnetic susceptibility provides alternative indicative information for ancient firing conditions in addition to conventional magnetic susceptibility. Furthermore, magnetic properties of burnt clay may decode the in-situ source characteristics with respect to geological background. In addition, a potential link between temporal variations in ancient firing temperatures in burnt clay and surrounding paleoenvironmental changes is tentatively interpreted by local environmental feedback of temperature-moisture conditions and anthropogenic activity. This study further confirms the archaeological potential of thermomagnetic properties as useful indicators in paleoenvironmental studies. More work combining paleoenvironmental and archaeological archives is critically essential to understand ancient firing history in the context of environmental conditions.

1. Introduction

The history of oxygen saturation in the atmosphere has led to the prevalence of fire as a fundamental element on Earth, resulting in

* Corresponding author. Guangdong Provincial Key Laboratory of Marine Disaster Prediction and Prevention, College of Science, Shantou University, Shantou, 515063, Guangdong, China.
** Corresponding author.
E-mail addresses: ligh1986@gmail.com (G. Li), gewei@xmu.edu.cn (W. Ge).

https://doi.org/10.1016/j.heliyon.2023.e20628
Received 7 July 2023; Received in revised form 3 October 2023; Accepted 3 October 2023
Available online 4 October 2023

widespread destruction and landscape changes caused by fires arising from various sources such as lightning strikes, volcanic ruptures, and spontaneous bio-ignition [1,2]. The use of fire by early hominins is considered a unique human capability that is of great importance in understanding the conscious use of fire and its role in the development of human civilizations [2]. Previous studies, combined with sedimentary and archaeological records, provided evidence of anthropogenic fire activity since at least the mid-Holocene period [3,4]. However, there is still no consensus on the temporal and spatial variations in human-controlled fire activities before the Industrial Revolution, possibly because of insufficient sedimentary and archaeological records for fire reconstructions [5,6]. Clay, as a moldable substance, could be hardened gradually by high-temperature grilling, which inspired early humans to invent pottery materials for construction [7]. Burnt clay, an ancient structural material commonly found in Neolithic remains, provides insights into ancient building techniques and the human use of fire [7–9]. The properties of historically burnt clay also contribute to the potential evaluation of renovation materials based on the chemical, physical, and mechanical behaviours of the ancient building systems [10]. Thermal treatments are commonly applied to recover the possible formation procedures and purposes of historically burnt clay materials within various architectures [10–12], yielding many methodologies for the assessment of ancient building materials [13]. The thermal formation and compositional alteration of burnt clay have recently become the focus of archaeological research, resulting in controversial debates because of the loose texture [8] and mineralogical complexity of most burnt clay remains [7,14]. To retrieve important information on ancient fires from burnt clay products, various methods, including infrared spectroscopy, Mössbauer spectroscopy, and X-ray diffraction have been used for mineralogical and elemental analyses during thermal treatments [7, 8]. These studies have made significant progress in the recovery of information on firing procedures, manufacturing technology, and environmental deterioration mechanisms. However, because of the complexity resulting from compositional differences, heat intensity, heat duration, and physical influences during treatment [7,15], additional approaches are required to further investigate burnt clays.

Rock magnetism is one of the most powerful tools for studying the magnetic behaviour and processes of natural and artefact materials under various geological conditions [16,17]. A precondition for rock magnetic analysis is the identification of the magnetic behaviours of natural magnetic minerals including ferromagnetic minerals such as magnetite, maghemite, and pyrrhotite, and incomplete antiferromagnetic minerals such as hematite and goethite [17]. These magnetic behaviours are mainly related to the magnetic mineralogy, magnetic crystal grain sizes and magnetic concentration, which reflect changes in the mineral preservation conditions. A comprehensive analysis of magnetic parameters could give rise to assessment of magnetic transformation affected by

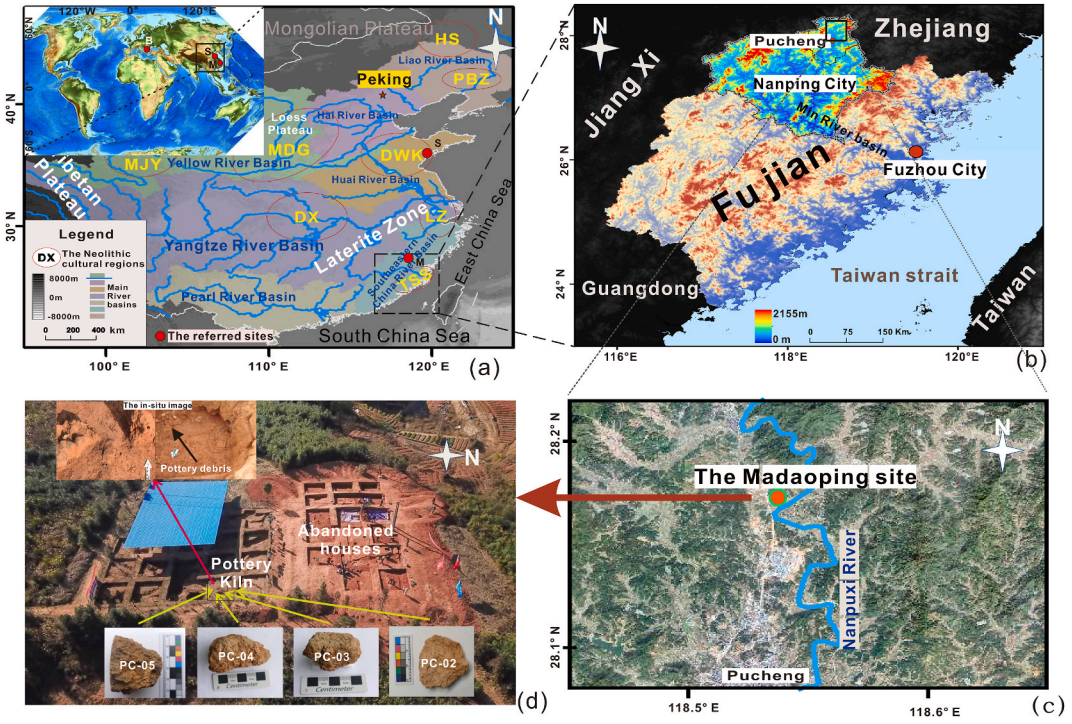

Fig. 1. (a) Map showing the relevant sites (B: Bulgarian burnt clay relics, S: Sujiacun burnt clay relics, M the Madaoping (MDP) relics) and Neolithic cultural regions in the context of main river basins in eastern China (HS, Hongshan culture. PBZ, Pianbaozi culture. DWK, Dawenkou culture. MDG, Madonggou culture. MJY, Majiayao culture. DX, Daxi culture. LZ, Liangzhu culture. TSS, Tanshishan culture). The dashed square indicates the location of Fujian province. (b) The topographic map of Fujian province showing the study area (the solid square) in the Min River basin. (c) The MDP site is located on the terrace of Nanpuxi river (one of the Min River tributary) as shown in the image (Google Earth). (d) The Photograph of excavation status in the MDP site where the burnt clay samples were collected in the southern part of excavated area. The yellow arrows denote the sampling positions and red arrows indicates the in-situ status of the burnt clay (also see the Supporting Information 1).

environmental changes [18]. Notbaly, the discovery of magnetic stability retention until the reburning temperature exceeds the original conflagration temperature provides a novel methodology for evaluating the firing history of burnt clay materials [19]. The alteration of magnetic minerals during natural and/or artificial combustion procedures under different redox conditions can cause changes in magnetic signals [17]. Thus, magnetic transformation with respect to redox reactions has been used to decode ancient firing conditions in Neolithic burnt clay from Eurape [19–21] and China [22]. However, magnetic alteration during burning not only leads to changes in magnetic mineralogy but also results in variations in magnetic concentration and grain size, as revealed by isothermal remanent magnetization (IRM) acquisition curves [23] and multiple magnetic properties [24,25]. Magnetic susceptibility usually contains more than one aspect of these factors and thus should be analyzed along with other magnetic and non-magnetic properties to elucidate ancient firing conditions. Recently, a combined study of magnetic and non-magnetic parameters was conducted on burnt clay specimens, revealing a direct link between magnetic characteristics and ancient firing temperature under various environmental conditions [26]. Such attempts have encouraged further advancement of magnetic approaches with a more comprehensive analysis of burnt clay materials in ancient ruins to explore crucial cultural information. Therefore, this study presents a systematic analysis of magnetic parameters to investigate ancient firing temperatures by stepwise thermal treatments of burnt clay specimens from a late Neolithic site in northern Fujian, southeastern China. Subsequently, cultural information obtained by combining magnetic and non-magnetic parameters is discussed. Additionally, this work focuses on the possible reason for the magnetic behaviors in burnt clay and the linkage between temporal variations in firing temperatures and paleoenvironmental conditions since the mid-Holocene period [26].

2. Materials and methods

2.1. Study area and samples collection

The Neolithic period was a pivotal period in human history that marked a profound transition from nomadic, hunter-gatherer societies to settled agricultural communities [27–30]. Over the last few decades, extensive archaeological excavations across various regions of China have unveiled remarkable Neolithic settlements as indicated in Fig. 1a, providing valuable insights into the rich tapestry of ancient Chinese cultures by their impressive infrastructure and intricate craftsmanship [29]. Previous archaeological investigations have revealed the onset of the Neolithic period dating back to approximately 18,000 BCE, as unearthed at Xianrendong Cave in China's Jiangxi Province [31]. However, notably, it took a substantial span of time, roughly between 8000 and 10,000 years, for the emergence of the earliest known villages among the late Palaeolithic hunter-gatherer communities inhabiting the regions of the middle and lower Yangtze [32,33]. There have been long debates about the termination of the Neolithic period in China, although most studies proposed a transition interval between 2000 BCE and 1500 BCE to the Bronze Age setting the stage for the Shang dynasty [29,34]. This estimation was reatively later than termination of the Neolithic period in certain parts of the Europe [35,36]. However, the ending of the Neolithic period in the Southeast China exhibit flourishing of relatively small-scale societies for a millennia after the emergence of early states and the onset of bronze production from the Yellow and Yangtze River basins in northern China [28]. A compilation of time line of prehistoric cultures indicate a period between 5050 BCE and 1550 BCE for the Neolithic occurrence in the southeastern China, to some extent marking the development of Neolithic cultures in Southesat China [28,37]. The study area (Fig. 1a and b) is located in northern part of Fujian province, southeast coastal area of China, geographically connecting the Yangtze River basin and the southeastern river basins, where the climate is characterized by a subtropical monsoon zone, with relatively warm and humid conditions throughout the year [38,39]. In 2018, relics of a Neolithic architectural complex (118.5° E, 28.0° N) were excavated in Pucheng, where the collapse accumulation and slope diluvium were widely distributed at the terrace surface of the Nanpuxi river (Fig. 1c). The site was approximately dated to the Late Neolithic period in Southesast China by radiocarbon dating (Table 1) and abundant pockmarked-stamped hard pottery fragments (Supporting Information 1). The site, hereafter referred to as the Madaoping (MDP) site, clearly reveals an ancient building assemblage with traditional Chinese settlement traits, consisting of two chamber groups, separated by a horizontal partition (Fig. 1d). Several burnt clay protrusions were spotted between the two chamber groups, and these burnt clay materials were regarded by archaeological identification as parts of an ancient kiln made of wood and mud mixtures. The kiln was located at the same cultural layer with the ancient building that was also dated back to the late Neolithic period in Southeast China (Fig. 1d). Several pottery debris pieces including sand pottery, clay pottery, and black pottery were spotted under the inner side of the kiln wall surrounded by the burnt clay materials. In addition, some burning ash remains were also found in certain layers of the ceramic-mixed soil (Supporting Information 1). The rising flame round kilns found at the MDP site were considered as the most complete late-Neolithic pottery kilns found in Fujian Province so far, which is of great significance to the study of the origin and development of southern kiln technology in southern China.

After removing the surface sediments, four sets of burnt clay unoriented bulk samples were collected by cutting blocks from the relics to ensure the integrality of the structure of samples. The burnt clay samples all consist of a greyish yellow part and a brownish red part (Supporting Information 1) to varying degrees, and the two parts of the representative sample PC-05 were also regarded as

Table 1
AMS^{14}C dating data of samples from the site profile in the MDP site.

Sample ID	Depth	Material	F^{14}C	σ- F^{14}C	^{14}C age (yr BP)	Cal.^{14}C age (cal.yr BP)
LZU23385	20–25 cm	Organic matter	0.8675	0.22	1140 ± 20	1020 ± 43
LZU23384	95–100 cm	Organic matter	0.6584	0.33	3360 ± 30	3591 ± 53

independent specimens in this study. The greyish yellow and brownish red parts are referred to as red and yellow parts, respectively, in the following sections. These samples were carefully wrapped by foamed plastic and silicon rubber case and packed in the glass box with gaps filled with foam plastic to reduce possible vibration and crushing during preservation and transportation. The samples were pretreated by removing the outer soils again by a ceramic knife after freeze drying in the laboratory for further measurements. In the laboratory, the bulk samples were subsequently cut into cube samples with a volume of 8 cm^3 by a ceramic knife, while the powder specimens were also collected for magnetic measurements.

2.2. Methods

Magnetic measurements were performed on the cubic specimens to examine the thermal alteration of magnetic minerals using related parameters. The ancient maximum firing temperature (T_{fire}) of the burnt clay in this study was determined by magnetic susceptbiliy (χ) variations [19]. Stepwise heating procedure for both bulk and powder samples was performed using a ASC Scientific (USA) TD48EU thermal demagnetization system from room temperature up to 780 °C.The thermal treatment was conducted by a 100 °C interval before 400 °C and subsequently followed by 450 °C, 500 °C, 580 °C, 620 °C, 680 °C, 720 °C and 780 °C steps. The heating duration for each step was set as 3 h before 500 °C and as 2 h after 500 °C before cooling down to room temperature. After each thermal treatment, the volume magneic susceptibility was measured at frequencies of 976 Hz (LF) and 3904 Hz (HF) in a field of 200 A/m using an AGICO multifunction Kappabrige MFK1-FA, Advanced Geoscience Instruments Company (AGICO), Inc, Czech Republic, with a sensitivity to susceptibility changes of 1×10^{-7} SI. Calibration of the bridge was performed every day before beginning the work with a calibration standard, and the value of the empty holder was measured after each calibration and subtracted from the sample values. Mass-specific magnetic susceptibility was then obtained by normalizing the volume susceptibility by each sample's mass, and the low frequency susceptibility was labelled as χ in the text. Frequency-dependent magnetic susceptibility in percentage form (χ_{fd}%) was calculated by the formula $\chi_{fd}\% = (\chi_{LF} - \chi_{HF})/\chi_{LF} \times 100\%$. Four samples were subjected to the χ-T treatment for T_{fire} determination. For the representative sample PC-05, the brownish red and greyish yellow parts were measured separately to assess χ-T variation differences between the two parts. Hysteresis loops, first-order reversal curves (FORC), isothermal remanent magnetization (IRM), back-field remanence and related parameters for the mixture of red and yellow parts of the representive sample PC-05 were measured at maximum field of 1T using a MicroMag 3900 Vibrating Magnetometer (AGM) (Princeton Measurements Corp., USA). The remanent magnetization at a 1T field is regarded as saturation remanent magnetization (Mrs). Unmixing analysis of the IRM acquisition curves was conducted based on the fitting of the IRM acquisition curve versus the logarithm of the applied field with the acquisition curve expressed as a gradient [40]. The optimal fit to a measured IRM acquisition curve was evaluated statistically using the smallest residual in relation to the number of magnetic components with different mineral coercivities. The distribution and mode fields largely represent the relative content and corresponding coercivity, respectilvey. The measurement of hysteresis loops and FORC curves also gives rise to saturation magnetization (Ms), coercivity (Hc), remanent coercivity (Hcr) and interaction field (Hu). Ms was obtained after exerting the 1T treatment in the presence of magnetic field, and the ratios of Mrs/Ms versus Hcr/Hc are commonly used in the Day plot for magnetic grain size assessment. The FORC diagram provides a means for determining the distribution of switching fields (Hc) and interaction fields (Hu) for all of the particles, thus distinguishing between SD and MD grains, as well as mixtures of different magnetic species during the thermal treatments [41]. For the representative sample PC-05, non-magnetic parameters were measured to analyze the differences between the red and yellow parts of the burnt clay. After being hardened and fixed on the microscope slide, polarizing microscope images of the bulk samples were acquired using a German Leica EZ4W stereoscopic microscope. Powder samples from the yellow and red parts of the representative sample were slightly ground. Specimens passed through a 100-mesh sieve (approximately 154 μm (μm)) were selected and placed into the sample holder for X-ray diffraction (XRD) measurements. The XRD measurements were performed for mineral analysis with a Bruker AXS D8 Discover X with a Cu target Kα radiation (=1.5406A), scanning Angle (2θ) ranging from 5° to 80°, and scanning speed of 5°/min. The detection of various mineral species and determination of the relative percentage content were completed using the MDI Jade software. Mineral determination was performed by comparing the position, intensity and number of diffraction peaks of the sample to be tested and those of the standard card based on SY/T 5163–2018 X-ray diffraction analysis for clay minerals and common non-clay minerals. Another group of fine powder specimens passed through a 200-mesh sieve (approximately 74 μm) was prepared by mixing 3.0g of the sample with boric acid powder and then forming rounded measuring wafer using hydraulic pressure equipment. Major element data were obtained by X-ray fluorescence (XRF) measurements using a Thermo Perform'X' Sequential Scanning XRF spectrophotometer. The XRF data were then corrected by calculating the theoretical strength of the X-ray lines, Loss on ignition LOI_{950}, and the sensitivity of elements through the standard samples refering to Chinese national standard soil samples including GSBZ50012-88, GSBZ50013-88, and GSBZ50014-88 [42]. The percentage of loss on ignition at 950 °C was indicated by LOI_{950}. The loss on ignition at 950 °C for two parts of the typical sample PC-05 were performed for XRF correction using KF-1200-I muffle furnace after 12h drying at 60 °C. Two samples from the upper and lower parts of the excavated trench profile in the MDP site were subjected to AMS ^{14}C dating with extractive organic matters. The samples were pre-treated by acid-base acid method and then measured using a 0.2 MV MICADAS accelerator mass spectrometry AMS^{14}C system (Ionplus AG, Switzerland). The AMS^{14}C data were processed according to the standard OXII 134.07pMC. The AMS ^{14}C ages were converted to calendar ages (Table 1) using the Calib 7.0.4 software program with the INTCAL 13 calibration dataset [43].

3. Results

3.1. Microstructural and geochemical characteristics of the burnt clay samples

The red and yellow parts of the typical sample exhibited a distinct appearance in color and porosity, as indicated in the microscopic images (Fig. 2a–c). The red region indicates a lower content of organic carbonaceous fragments and more porous structures. The transition part reveals a significant distinction between the brownish-red and the greyish-yellow parts, indicating an oxidizing condition with a relatively longer sintering duration in the red part than that in the yellowish section. As shown in Fig. 2, the slightly developed porosity in the red part may indicate an intensified firing process, during which organic materials and calcite fractions were potentially consumed by the combustion to form a large area of pores [44]. Fig. 2d–e illustrate the clay mineral analysis in the red and yellow parts, respectively, showing a homogeneous composition mainly including quartz, albite, orthoclase, muscovite and hematite. The absence of mullite in the samples may denote a firing process without exceeding 1000 °C [45]. The chemical composition changes (Fig. 2f) revealed that both the yellow and red parts contain relatively high amounts of SiO_2, Al_2O_3, and Fe_2O_3 and low amounts of chemically active elements, such as K_2O, MgO, Na_2O and CaO in decreasing order, which is similar to the record from nearby soils [46, 47]. This may suggest the dominance of geochemical signals from regional sediment weathering. The contents of SiO_2, Fe_2O_3, TiO_2, MgO, and CaO were slightly higher in the yellow part than those in the red part, whereas other elements showed higher contents in the red part, implying possible alteration during or after the firing procedures.

3.2. Magnetic properties of the burnt clay samples

The magnetic properties of the representative sample PC-05 during thermal treatments are illustrated in Fig. 3. The values of χ in both yellow and red parts varied from 80 $\times$ $10^{-8}m^3kg^{-1}$ to 200 $\times$ $10^{-8}m^3kg^{-1}$ along with rising temperatures, and the χ and χ_{fd}% curves in the two specimens shared similar variation trends in general. Typical hysteresis loops during heating show a generally narrow

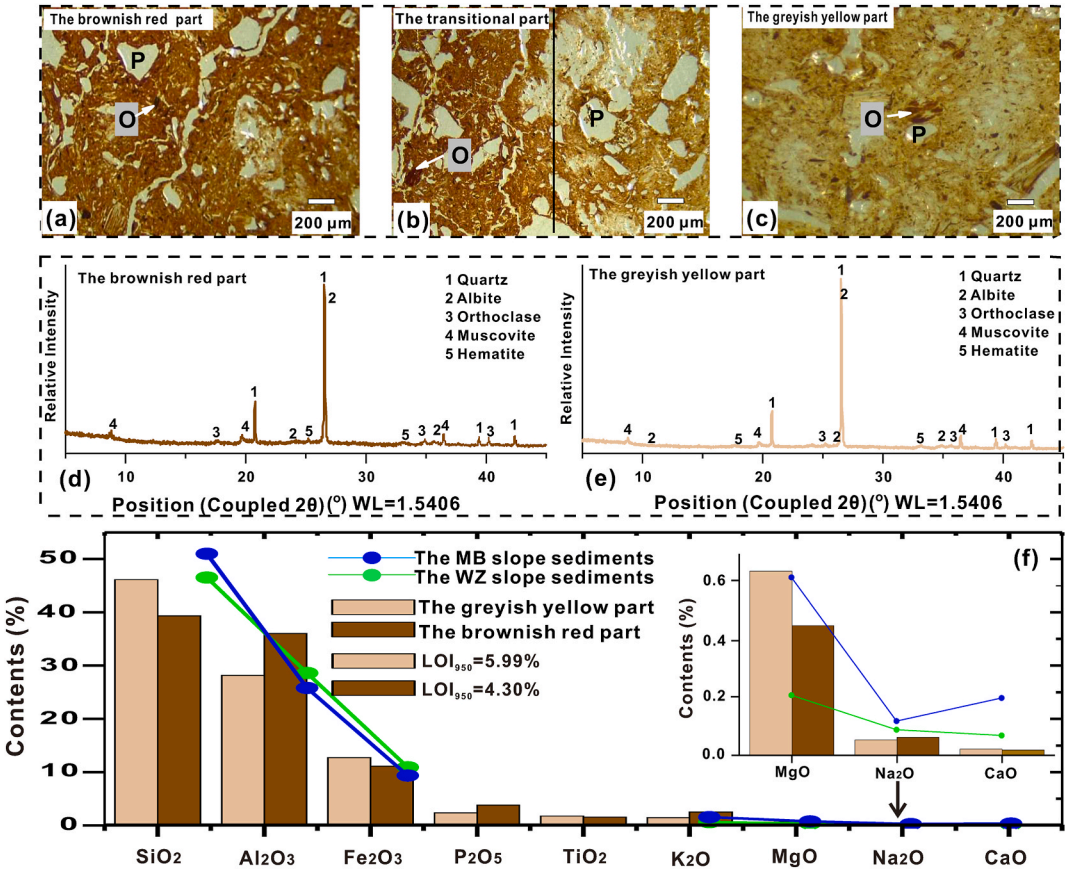

Fig. 2. (a–c) The microscope images from the red and yellow parts, respectively, of the typical sample PC-05. The pore structures (P) and organic material remains (O) are indicated. (d–e) Mineralogical compositions of the two parts from the sample PC-05. Peaks correspond to each identified crystalline phases. (f) Histogram of elemental composition of the two parts from the sample PC-05 in comparison with records from the WZ and MB slop sediments in adjacent area [47]. The inset manifests elemental composition with low contents. The elemental composition of the two parts was corrected according to LOI after 950 °C treatment.

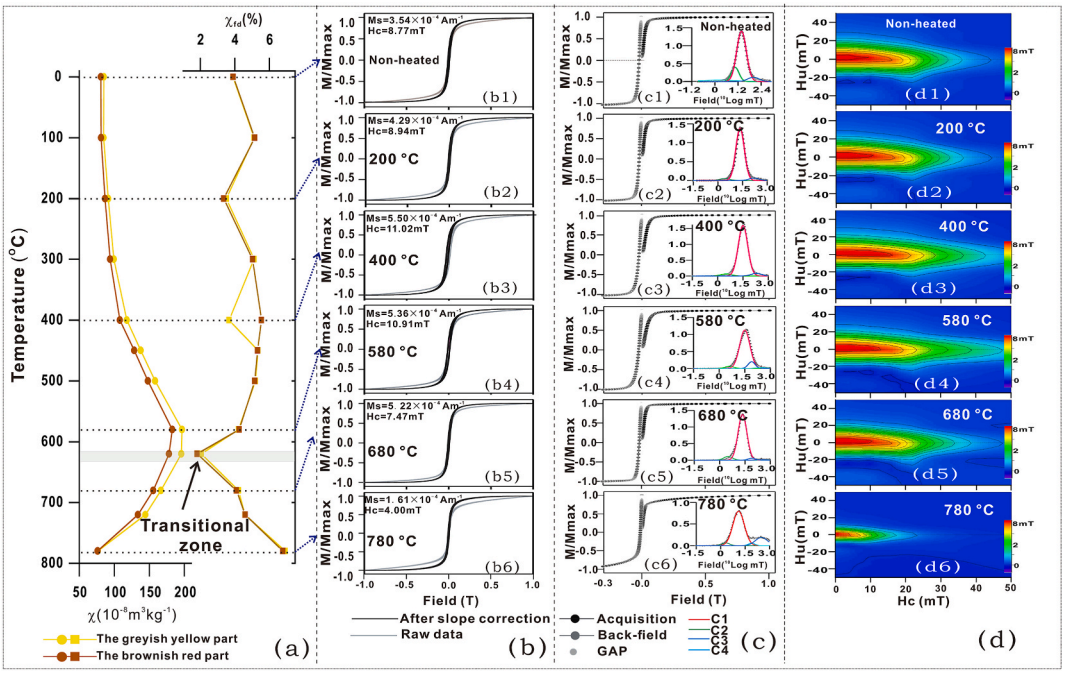

Fig. 3. Magnetic properties of the representative sample PC-05. (a) Variation of χ and χ_{fd}% of the yellow and red parts from the PC-05 sample after heating steps; (b) Hysteresis loops of the sample with mixture of red and yellow parts from the PC-05 sample; (c) The IRM acquisition and back-field remanence curves along with unmixed fractions of the IRM acquisition using IRM-CLG program with the gradient acquisition plot (GAP) by Kruiver et al. (2001) Ref. [40]; $Cx_{(1\text{-}4)}$ indicates the unmixed magnetic components. (d) FORC diagrams for the PC-05 sample after heating steps.

loop type, revealing the dominance of pseudo single domain (PSD) magnetite [17] (Fig. 3b). There were basically three types of unmixed Hcr components of IRM acquisition, the modes of which were 4 mT, ca. 25 mT and more than 158 mT (Fig. 3c). The FORC diagrams [41] demonstrate closed peak structures and coercivity spectra centered at about 20 mT, implying the dominance of PSD magnetite in the samples (Fig. 3d). The enlargement of the contours near the applied field axis (Hu) and the central ridge along the Hc-axis indicates an underlying contribution of feebly interacting single domains (SSD) or superparamagnetic (SP) particles [48]. The FORC distribution after 780 °C becomes very close to the Hu axis, suggesting the possible influence of hematite with a Curie temperature at 675 °C [17,49].

Day plot has been widely applied as an effective method to distinguish magnetic grain sizes in natural and artefact samples based on the ratio of saturation remanence to saturation magnetization, Mrs/Ms, against the ratio of remanent coercive force to ordinary

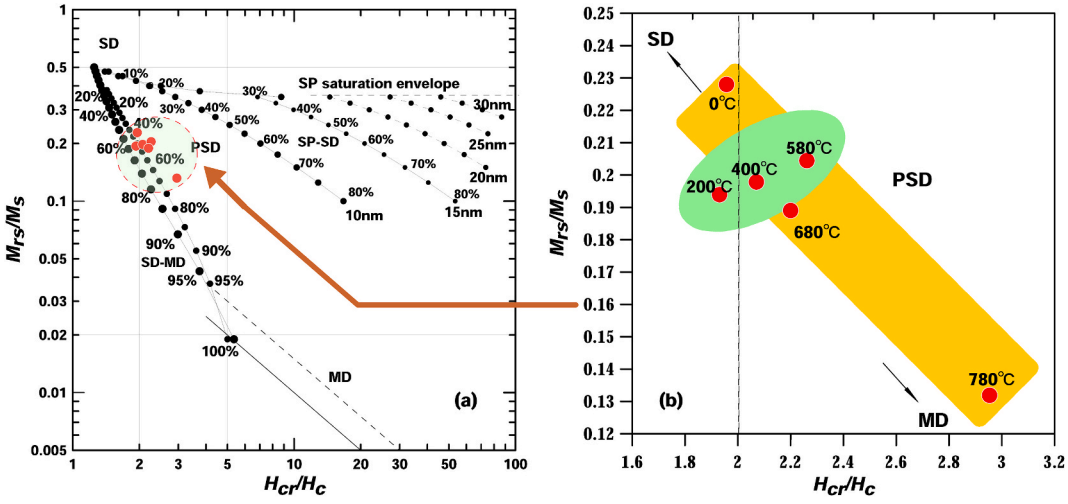

Fig. 4. Day plots of the mixture of red and yellow parts from the representative sample PC-05 after each heating process. (a) Day plot of the sample through stepwise thermal treatments compared to theoretical mixing curves [51]; (b) Day plot zooming in to focus on the data section.

coercive force, Hcr/Hc [50,51]. The Day plot of the representative sample after each heating step is shown in Fig. 4a, and all data are bracketed within the PSD domain state along the SD-MD mixture grain line. According to theoretical calculations [51], the data were plotted within the domain state at approximately 50% MD-SP volume fraction in mixtures with SD grains. Fig. 4b illustrates the detailed inspection of data after different heating temperatures, showing a general descent in Mrs/Ms towards the MD domain state with an increased temperature owing to possible reduction of fine magnetite particles as also revealed in χ_{fd}%. Notably, there was an increasing trend in Hcr/Hc between 200 °C and 580 °C, while the data for heating between 680 °C and 780 °C are obviously influenced by hematite nucleation during firing. Together with the increase in Hc in the hysteresis loops, this could be postulated to be an alteration of ferrimagnetic minerals, leading to hematite nucleation during firing that is in line with the IRM and FORC analyses.

4. Discussion

4.1. Assessment of firing temperatures in the neolithic burnt clay based on magnetic approaches

As depicted in Fig. 5, χ values of all samples exhibit similar patterns of variation. These patterns were characterized by stable variation before approximately 300 °C, an increasing trend between 300 °C and 620 °C and a distinct decrease after 620 °C. This variability is in line with the variation in Hcr and Mrs of the representative sample shown in Fig. 5a3, indicating an unblocking or newly formed magnetic component with relatively high coercivity between 300 °C and 620 °C [52], as also revealed by FORC diagrams in Fig. 3d. The χ_{fd}% values of all the samples varied from 2 to 6, indicating a multiple compounds of magnetic grain sizes with moderate concentrations of SP particles [53]. Considering the decreasing trend of Mrs, enhanced χ_{fd}% values after 620 °C may suggest the finer alteration of strongly magnetic minerals (like magnetite) and hematite nucleation causing low remanence and reduced remanent coercivity (Hcr) [21]. The weak magnetic signal after high temperatures above 620 °C is further confirmed by the FORC diagram as illustrated in Fig. 3d6. Therefore, magnetic analysis largely manifested a significant transition temperature point at around 620 °C in all burnt clay samples from MDP site. In this study, assessment of ancient firing temperature maximum (T_{fire}) was conducted according to the most conservative criteria for evaluating the threshold firing temperature, in which the first noticeable increase in the $(d\chi/dT)^2$ was primarily taken into consideration along with the variation in other magnetic parameters [19,21]. The results as shown in Fig. 5, indicate that a stable magnetic variation pattern upon heating in all samples, exhibiting prominently high χ, Mrs and Hcr values at the heating temperature of 620 °C, corresponding to an obvious depletion of SP particles as indicated by χ_{fd}%. When the heating temperature exceeds 620 °C, the significant change in magnetic parameters would probably result from magnetic transformation beyond the T_{fire}. Moreover, for the two parts of the PC-05 sample (Fig. 5 a1-a2), there were two explicit variation transitions in the $(d\chi/dT)^2$ curves located at about 400 °C and 620 °C, respectively, and the prominent transition temperature at around 620 °C could be easily identified in PC-04 and PC-05 samples. The other two samples PC-02 and PC-03 present a relatively distinct transition point of the

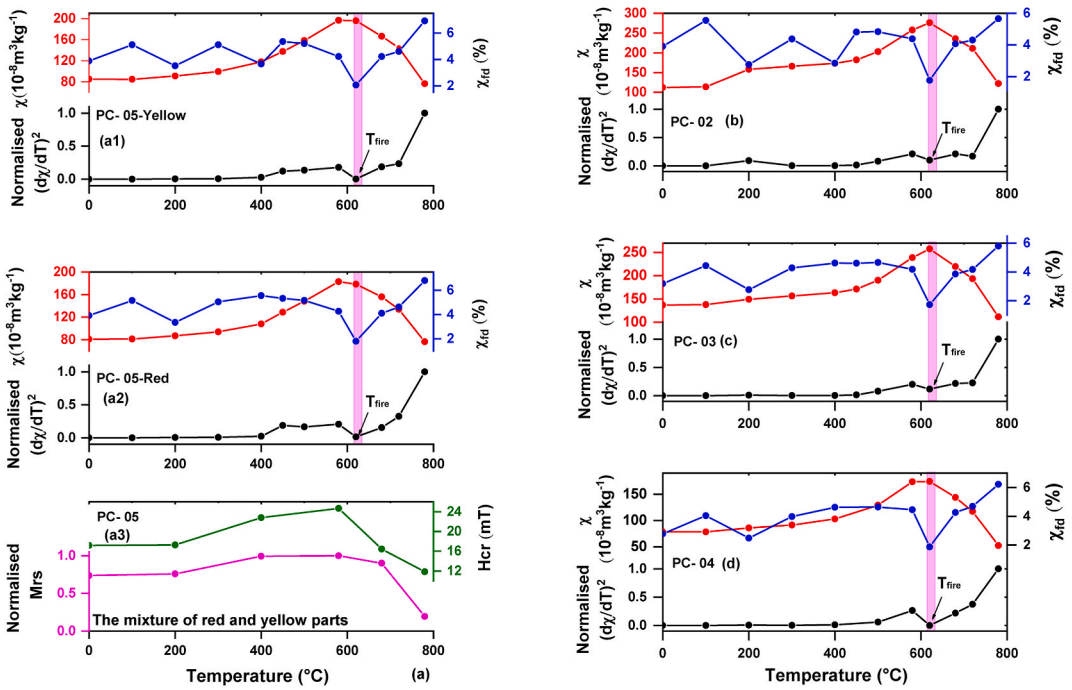

Fig. 5. Determination of the T_{fire} based on magnetic variation of burnt clay materials in MDP site including χ, χ_{fd}%, Mrs and Hcr at room temperature after each laboratory heating step from ambient to 780 °C. The Mrs and $(d\chi/dT)^2$ values are normalized by their maximum value. The pink bars indicate the T_{fire} determination in each sample.

$(d\chi/dT)^2$ at 720 °C and a relatively moderate transition at about 620 °C. The first large deviation of the $(d\chi/dT)^2$ is not consistent with abrupt magnetic susceptibility transitions as indicated in Ref. [19]. Notably, χ_{fd}% variation gives rise to prominent change of SP particles at 620 °C in these samples, also corresponding to the moderate $(d\chi/dT)^2$ transition, suggesting that the maximum ancient firing temperature has been reached [24]. Thus, the T_{fire} of burnt clay samples at the MDP site was essentially constrained at 620 °C, after which magnetic signals varied significantly as a result of drastic magnetic phase transformation based on χ and χ_{fd}% variations.

The formation and building purpose of burnt clay relics still remain controversial, and several hypotheses have been linked to conscious combustion or baking [22] and accidental firing [54,55]. Based on comparative analysis of natural fire and human controlled fires, which suggests a limitation of no more than 400 °C for natural burning [56], the ancient firing temperature confined to approximately 620 °C in this study hardly indicate casual combustion in burnt clay materials. An accidental fire usually causes uneven inflammation that results in unconformable clay blocks with uneven color and unburnt carbonized vegetation remains [54]. As illustrated in Fig. 2, there was no obvious evidence of large-carbonized plant remains in the images despite the pore structures. Human controlled fires may possibly be responsible for the formation of burnt clay materials at the MDP site. The T_{fire} at approximately 620 °C is also in good agreement with other evidence based on magnetic approaches from other civilized areas during the Neolithic period [14,21,22]. During field work, the burnt clay materials are located apart from the ancient domicile, where no significant conflagration was observed (Fig. 1). Meanwhile, the shape of the relics resembled a kiln chimney wall with obviously harderned burnt clay that clearly distinguished from the surrounding loose laterite (Supporting Information 1). Considering the numerous pieces of pottery debris within the relics, the burnt clay materials in this study were presumed to be a consequence of a discarded pottery kiln. Nevertheless, previous analysis in the pottery kiln presented more than 850 °C firing temperature which is much higher than the determined T_{fire} in this study [57]. The distinction of elemental compositions and granulometric records between the red and yellow parts of the burnt clay also supports the relatively limited heat penetration during ancient firing (Fig. 2), although it is possible that some parts of the initial material were not crushed enough to be flammable, resulting in differences of post-firing characteristics in different parts of the burnt clay. Considering the colour and density differences between the inner and outer parts of the in -situ burnt clay, we tentatively deduce that the burnt clay materials possibly belonged to the inner part of an abandoned enclosure probably connecting to the kiln for temporary pottery storage due to the presence of certain pottery fragments within the enclosure (Fig. 1 and Supporting Information 1). Therefore, it would be reasonable to assume that the burnt clay was used as construction materials through a humanly controlled firing for preservative storage in the kiln.

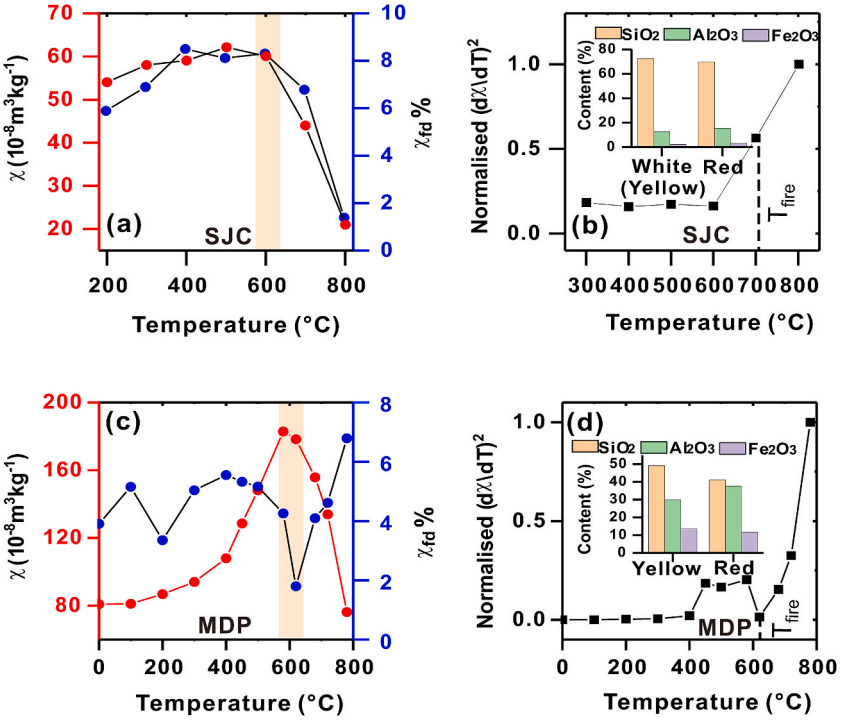

Fig. 6. Comparison of magnetic susceptibility records associated with the T_{fire} determination of the red part of the burnt clay materials between the Sujiacun (SJC) site [22] (a–b) and the MDP site (c–d) in this study. For the MDP site, magnetic data of the red part and elemental data from the representative sample PC-05 are presented (c–d). The $(d\chi/dT)^2$ values are normalized by the maximum value. The inset illustrates the elemental distinction of the red and yellow parts of the burnt clay between the two sites.

4.2. Geological imprints of the ancient firing in the burnt clay

The T_{fire} of burnt clay materials is highly variable because of the possible influence of the local clay source, which may be preliminarily embodied in compositional variations [26,58,59]. Compositional differences in burnt clay from various regions largely stem from the geological setting of clay sources and architectural purposes [21,59]. This study compared magnetic behavior of burnt clay materials from the MDP site in this study with that from Sujiacun site with respect to the T_{fire} recovery (Fig. 6a–d). The Sujiacun site generally dated back to the early Longshan Culture (approximately 2500 BCE) is located in an area with brown soil distribution in northern China and is in distinct contrast to the MDP site in southeastern China [22], which features laterite soil. The burnt clay

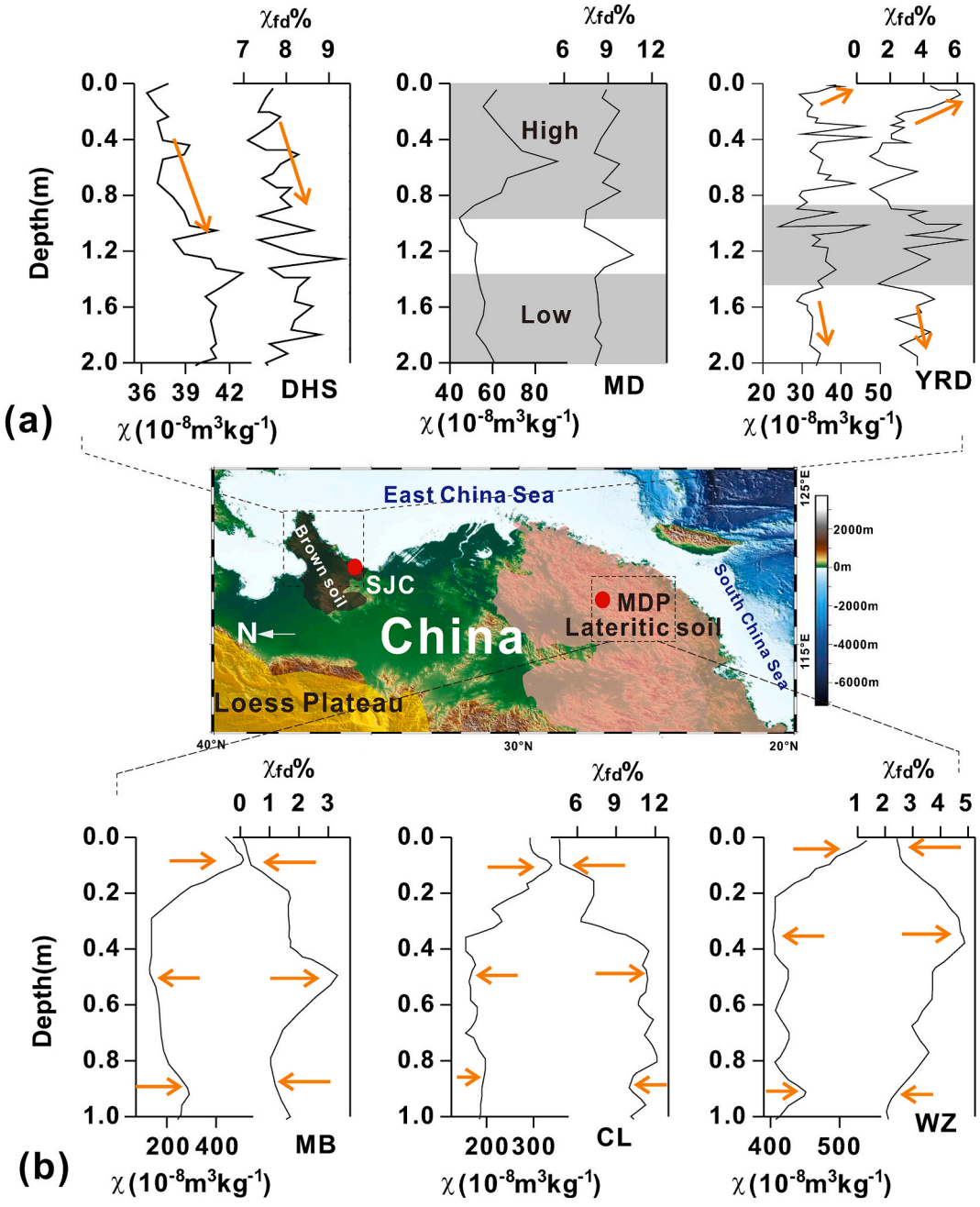

Fig. 7. (a) The reference records of χ and χ_{fd}% from sedimentary sites close to the Sujiacun site in the northern China [66,67,69] and (b) the MDP site in the southern China [47], respectively. DHS: Daheishan section [67]; MD: Miaodao loess section [69]; YRD: Sediments from Yellow River Delta [66]; MB: Mabao section [47]; WZ: Wuzhai section; CL [47]: Changle section [47]. The grey area and orange arrow indicate the variation of χ and χ_{fd}% in the sections.

samples from Sujiacun site exhibit two marked colors, namely red (brownish red) and white (greyish yellow) parts, which are similar to those found at the MDP site [22]. Although magnetic approaches revealed high similarity in the T_{fire} record at approximately 620 °C in burnt clay from both Sujiacun and the MDP sites, the variation pattern of magnetic susceptibility showed distinct differences. The burnt clay sample from Sujiacun site exhibited lower variability of magnetic susceptibility until 600 °C [22], suggesting a comparatively depressed transformation of iron-bearing silicates in the Sujiacun sample. This inference is largely consolidated by evidence from the major element analysis in Fig. 6b and d, which shows a relatively limited change in the major element content between the yellow and red parts of the burnt clay from Sujiacun site. Notably, laterite contains more than 10% of Fe_2O_3, which gives so intense reddish color for the MDP site and intensifies the redness of the brownish red part during firing [60]. Additionally, there was a reverse variation pattern between χ_{fd}% and χ in the burnt clay samples from the Sujiacun site and the MDP site. The contribution of superparamagnetic fractions to total magnetic susceptibility has been proven to be a prevailing reason for magnetic enhancement in many sediments, including archaeological deposits [61,62]. This interpretation is suitable for the Sujiacun burnt clay samples [22]. However, the MDP record might be an exception to this relationship (Fig. 6c) because the intense oxidation possibly exceeded a critical threshold under relatively warm and humid conditions, causing more hematite to suppress the contribution of SP particles to magnetic enhancement [18,21,63]. When the heating temperature exceeded 400 °C, an opposite trend between χ_{fd}% and χ was explicitly observed in the burnt clay samples from the MDP site and magnetic depletion in high temperature heating would possibly result from the transformation of strong magnetic minerals (such as magnetite) to weakly magnetic fractions (like hematite) [17,21] as also indicated in Fig. 3. During heating processes, magnetite surface reacts with oxygen to first form the Fe^{2+} cation deficient phase γ-Fe_2O_3 (maghemite), and then be further oxidized to form hexagonally-close-packed α- Fe_2O_3 (hematite) [64]. Consequently, compared with the Sujiacun burnt clay record, the possible thorough oxidation during high-temperature heating may have resulted in a high concentration of SP hematite

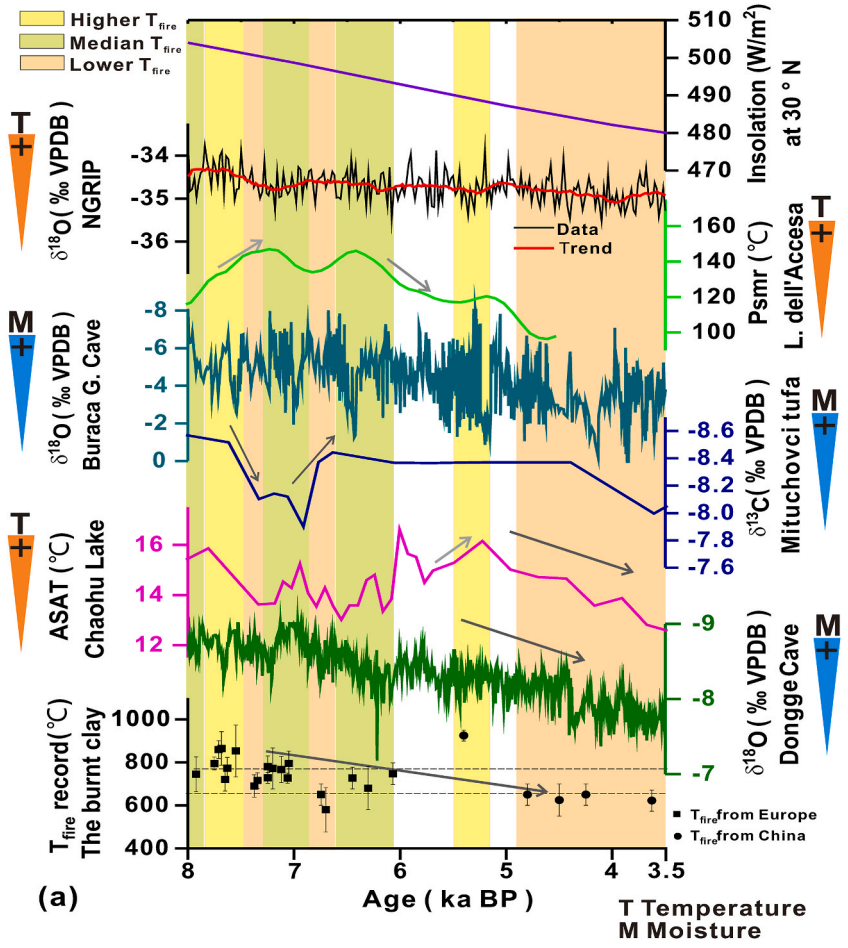

Fig. 8. Comparison of the T_{fire} records from eastern China [22,75] and Bulgaria [26] with regional and global paleoenvironmental records during the Neolithic between 8.0 ka BP and 3.5 ka BP, including $\delta^{18}O$ time series of the Dongge Cave [76], air temperature reconstruction from the Chaohu lacustrine sediments [78], a European stalagmite $\delta^{18}O$ from Portugal [71], a tufa calcite record of the Mituchovci site, Carpathian Mountains, Slovakia [72], a pollen record from Italy [74] and $\delta^{18}O$ record from Greenland (NGRIP) [80]. The summer insolation at 30° N was also presented as a driven reference of global temperature variations [81]. The black arrow outlines the general trend of paleoenvironmental proxy variations while the red line indicates the T_{fire} in this study.

(Fig. 6a and c), which has also been reported as a result of color differences in other burnt clay studies [7,21].

Moreover, the local circumstances at the MDP site in the laterite zone of southern China were quite different from those at the Sujiacun site in the loessic-brown soil zone of the northern China (Fig. 7). In the latter case, a generally covarying trend similar to certain records from the Loess Plateau [62,65] was observed between χ_{fd}% and χ in the upper part of sediments from Shandong peninsula close to the Sujiacun site (Fig. 7a). On the contrary, magnetic characteristics of the late Pleistocene laterite also revealed largely antiphase relationship between χ_{fd}% and χ in the upper segments (possibly the Holocene epoch), which is generally similar to the burnt clay records in this study [47] (Fig. 7b). Magnetic assemblages in soils are primarily controlled by local parent materials and pedogenic processes that affected the formation and transformation of magnetic minerals [17]. Sediments in the Shandong Peninsula generally originated from dust transportation from western deserts and nearby shelves, and from fluvial materials in temperate zones [66,67]. The source materials and local situation might benefit the preservation of fine magnetite in the soils, including those used for burnt clays as indicated by covarying trend between χ_{fd}% and χ. The variation of fine SP magnetite contributed to magnetic susceptibility causing covarying pattern between χ_{fd}% and χ [22]. In contrast, laterite soils in south China are derived mostly from the weathering of local bedrocks and fluvial origin from regional area under subtropical conditions [47,63,68]. The degradation of χ and enhancement of χ_{fd}% were believed to be pedogenic transformation of maghemite to hematite due to strong oxidation conditions [63,68]. Consequently, the local geological background exerted an important effect on the magnetic composition of burnt clay materials during ancient construction and on magnetic transformation during heating.

4.3. *Paleoenvironmental imprints of the ancient firing in the burnt clay*

Recent studies have suggested that the estimated average T_{fire} values were higher in Early Neolithic sites than those in Late Neolithic sites in Europe, and this difference was hypothetically attributed to differences in climate regimes or differences in the vegetation-related fuel used in house construction and the intentional burning of Early Neolithic houses [26,58]. As shown in Fig. 8, the average T_{fire} determined from Neolithic sites in both China and eastern Europe demonstrates a decreasing trend from the early to middle Holocene. For the temporal variability of the burnt clay T_{fire} from Bulgaria and Greece, the higher T_{fire} record was relatively confined between approximately 8.0 ka BP and 7.5 ka BP, which was previously included in the increased fire period in the early Holocene [70]. Moreover, the recent stalagmite records from the western Iberia, Portugal [71], and paleoclimate reconstruction in a

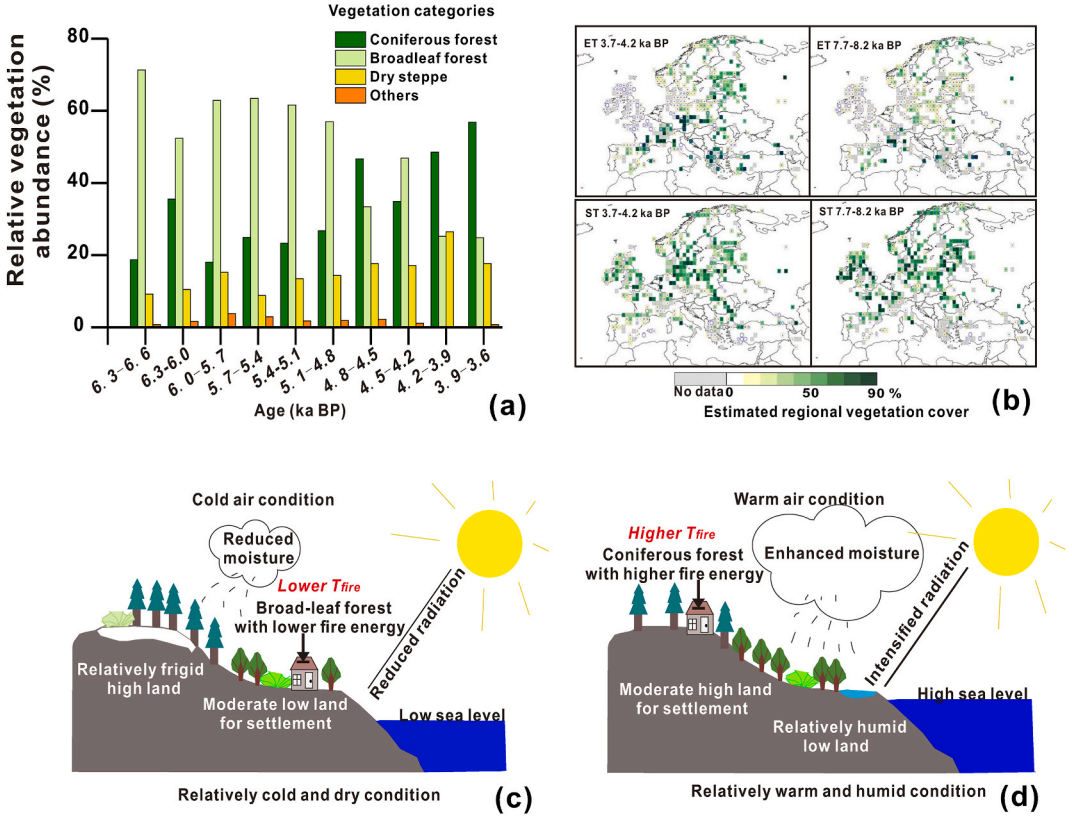

Fig. 9. (a) Relative vegetation abundance reconstructions from the monsoonal area in eastern China [84]. (b) Grid-based estimates of evergreen tree (ET) cover and summer-green tree (ST) cover for two relevant Holocene time windows in Europe [83]. (c–d) Assumed conceptual model for interpreting the T_{fire} records of burnt clay materials in the Chinese Neolithic relics associated with anthropic settlement adoption under paleoenvironmental conditions around 5.5 ka BP and 4.5 ka BP, respectively.

tufa deposit from Western Carpathians (Slovakia) [72] disclosed moisture variations from a relatively humid interval between 8.0 ka BP and 7.5 ka BP and a relatively dry interval around 6.8 ka BP, consistent with the climate-driven vegetation alteration at 7.5 ka BP in the northwestern Mountains in Bulgaria [73]. Furthermore, the Italian lake sediments decoded a Holocene paleoclimate record denoting a humid and overall increasing temperature between about 8.0 ka BP and 7.5 ka BP [74]. Subsequently, only two data with low T_{fire} were confined at the time interval around 6.8 ka BP, coinciding with a distinct temperature drop in the Italian lake sediments and relatively dry interval in the stalagmite records [71,74]. During this period, moisture record from the Carpathians showed an increasing pattern with a feeble slope variation in the $\delta^{13}C$ curves due to possible limited resolution and mountain conditions [72]. Notably, there was a relative enhancement of T_{fire} with a deceasing trend ranging from 6.0 ka BP to 6.5 ka BP, corresponding to relatively incremental humidity and enhanced temperature in this period. The data from Lingjiatan site dated around ca. 5.4 ka BP with high T_{fire} were prominently correlated with an increasing temperature and moisture in the southern China [75]. Additionally, the declining trend of T_{fire} in China is, to some extent, a response to humidity variations driven by a decline in Asian monsoon intensity and decreasing air temperature in southern China [76–79]. Therefore, a possble link between paleoenvironment changes and the T_{fire} variations of burnt clay might have somewhat become clear over the time interval at least between ca. 8.0 ka BP and ca. 3.5 ka BP covering the middle and late Holocene in both Chinese and European records, with the lower T_{fire} corresponding to relatively cold and arid periods.

It has been suggested that timber density, species, and moisture content are important factors influencing the structural performance of timber in fire [82], and burnt clay materials with the incorporation of pine wood provide more energy for fuel than oak wood [26,82]. Recent vegetation reconstructions in monsoonal areas of China and Europe presented a relative increase in coniferous evergreen tree (ET) forest cover with a decrease in the broadleaf summer-green tree (ST) forest abundance during the mid and late Holocene [38,83,84] (Fig. 9a–b). Considering the burning energy differences between thermophilic and hardy vegetations, the natural adoption of dominant vegetation can hardly explain the lower T_{fire} from both Chinese and European records. Thus, changes in the vegetation gradient in mountain areas in the context of the adoption of human settlements related to environmental variation should be considered. Evidence from Bulgaria presents a distribution tendency of high T_{fire} values for relics located at high altitudes before about 5500 BCE [26]. Similarly, Archaeological investigations in China have revealed that settlements during the Early Chinese Neolithic period were predominantly located on river terraces or in mountainous areas at high elevations [85,86]. During the Middle to Late Neolithic period in China, settlements were primarily situated near the main stem of rivers at lower elevations [85,86]. Anthropogenic activities expanded to areas closer to the ocean because of the relatively cold and dry climate with a drop in sea level after 5.0 ka BP [85]. Consequently, a hypothetical interpretation (Fig. 9c–d) for temporal T_{fire} variations both in eastern China and Europe appears to be the optimization of interactions between human controlled fire activities and paleoenvironmental changes [26, 59,70], although intentional firing behavior by an additional supply of fuel causing extensive combustion during Early Neolithic would be possible as well [14]. The relatively high air temperatures, along with high moisture conditions would largely facilitate vegetation prosperity and the high land expansion of anthropogenic activity, which may possibly benefit coniferous timber selection for construction and fuel during ancient firing [59,76]. The high T_{fire} during relatively warm and humid periods around 7.5 ka BP in Europe and 5.5 ka BP in monsoonal South China is assumed to be a consequence of human habitation adoption at higher altitudes and fuel option for coniferous timbers with relatively higher energy. On the contrary, a relatively arid and cold condition around 6.8 ka BP in Europe and 4.5 ka BP in China probably impelled the usage of broad-leaf timber in lowland areas due to the frigid circumstances at higher land, giving rise to the lower T_{fire} in the burnt clay. Furthermore, warmer air temperatures during the Early and Middle Holocene (Fig. 8) could have potentially enhanced the maximum firing temperature of burnt clay materials [70]. A recent comprehensive evaluation of the Holocene global temperature conundrum also confirmed that the global average temperature approximately 6.5 ka ago was likely warm followed by a multi-millennial cooling trend that ended in the 1800s [87]. The reducing trend of solar radiation and global temperature revealed through isotopic records from NGRIP (Fig. 8) from 8.0 ka BP to 3.5 ka BP may potentially bring about the overall reducing trend of the T_{fire} records in the burnt clay in addition to moisture changes. Nevertheless, local conditions in relation to temperature-moisture combination are speculated to have a pivotal impact on ancient firing temperatures because of good correlation between the T_{fire} records and local paleoenvironmental changes in details. This scenario would be more explicit if more work concerning T_{fire} at different altitudes are sufficiently supplemented [26].

There is also a clear difference of human acitivities between the burnt clay from this study and that from Bulgarian sites, although certain Neolithic relics from both China and Bulgaria were assumed to originate from deliberate burning [14,75]. The Bulgarian burnt clay was obtained from sites which were destroyed by fire mainly controlled by the external environmental conditions [14,26]. However, the burnt clay in this study was derived from the pottery kiln relics, where more interference would have been exerted by human activities during the controlled combustion. The difference of the archaeological structures and function of burnt clay materilas would possibly have affected the paleo-fire sensitivity to the surrounding environment. Moreover, the temporal variations of the T_{fire} records would potentially be influenced by the dating uncertainty of archaeological sites from different areas. Therefore, how and to what extent did the archaeological properties of the relics affect paleoenvironmental imprints of ancient fire in burnt clay should be further clarified in the furture. More relevant data and additional work combining paleoenvironmental and archaeological archives are critically essential for constraining ancient firing history in the context of paleoenvironmental changes during the Holocene epoch.

5. Conclusions

The Neolithic burnt clay was broadly distributed in archaeological relics of ancient civilizations across the Eurasian continent, providing key materials for understanding the firing history in ancient civilizations. This study contributes a late Neolithic burnt clay-based record of firing temperatures in relation to paleoenvironmental conditions from southeastern China. Based on magnetic and non-

magnetic analysis, firing temperatures and its environmental imprints of the burnt clay materials were assessed. The main conclusions from the study follow:

(1) The magnetic properties of burnt clay materials are dominated mainly by ferrimagnetic minerals, such as magnetite and maghemite, as well as incomplete antiferromagnetic minerals, such as hematite, which exhibit a pseudo single domain state. The non-magnetic characteristics revealed subtle differences in composition, porosity, and organic remains in different parts of the burnt clay, which exerted limited effects on the magnetic properties. This suggests that the fire process was likely controlled by humans. High-temperature combustion results in increased hematite fractions and can lead to irrelevant or even opposite variations in the magnetic concentration and superparamagnetic content.
(2) The ancient maximum firing temperature at 620 °C was determined, which is comparable to coeval records in China. In addition to conventional magnetic susceptibility, frequency-dependent magnetic susceptibility provides indicative information for determining ancient firing. Magnetic records are likely to be affected by the in-situ source of the burnt clay. The heating processes for burnt clay materials from the lateritic zone could possibly produce more SP hematite rather than fine magnetite, which contributes more to the enhancement of the magnetic concentration in burnt clay from brown and loessic soil areas.
(3) This study suggests a possible link between the temporal distribution of ancient firing temperatures in burnt clay materials and surrounding paleoenvironmental changes in both European and Chinese records. Regional moisture changes and anthropic adoption activity driven by paleoenvironmental conditions, including precipitation and temperature fluctuations, may be primarily responsible for the temporal variation of ancient firing temperatures between 8.0 ka BP and 3.5 ka BP. This study also has implications for the thermomagnetic properties of burnt clay as useful indicators in paleoenvironmental studies. Thus, it potentially contributes to the further conservation and renovation of cultural relics under specific environmental conditions. Nevertheless, further work combining paleoenvironmental and archaeological archives is critically essential for understanding ancient firing history.

Data availability statement

Data associated with this study are included in article/supp. Material/referenced in article.

CRediT authorship contribution statement

Guishan Chen: Methodology, Software, Writing – original draft, Investigation. **Guanhua Li:** Conceptualization, Formal analysis, Funding acquisition, Investigation, Methodology, Supervision, Writing – review & editing, Validation. **Miaomiao Liu:** Methodology, Software, Investigation, Visualization. **Wei Ge:** Data curation, Investigation, Resources. **Guibin Wu:** Data curation, Resources. **Changfa Zhan:** Funding acquisition, Supervision.

Declaration of competing interest

The authors declare that they have no known competing financial interests or personal relationships that could have appeared to influence the work reported in this paper.

Acknowledgements

The authors are indebted to Miss. Xiaohan Dong from Southern Marine Science and Engineering Guangdong Laboratory (Zhuhai), Miss. Sijing Zheng from Sun Yat-sen University, Mr. Jianye Li from Lanzhou University and Mr. Yubo Yang from Guangzhou Tuoyan Analytical technology for the laboratory assistance in this study. We are grateful to the Associate Editor Prof. George Iliopoulos, Dr. Jairo Martínez and the two anonymous reviewers for detailed and constructive comments and suggestions which helped to improve the manuscript. Special gratitude should be given to Prof. Erwin Appel for valuable comments and suggestions. We are also grateful to the field work groups from Xiamen University and Pucheng Museum who helped with sampling and archaeological documentation. The authors also thank Mr. Garrett Thompson from the Translation Department in the School of International Studies, Sun Yat-sen University for the language corrections. This study was financially supported by the National Natural Science Foundation of China [grant number 41704069], Southern Marine Science and Engineering Guangdong Laboratory (Zhuhai) [grant number: SML2020SP006] and the STU Scientific Research Start-Up Foundation for Talents [grants: NTF21025].

Appendix A. Supplementary data

Supplementary data to this article can be found online at https://doi.org/10.1016/j.heliyon.2023.e20628.

References

[1] A.C. Scott, Fire: A Very Short Introduction, Oxford University Press, 2020. https://books.google.com.hk/books?hl=zh-CN&lr=&id=GSvsDwAAQBAJ&oi=fnd&pg.
[2] S.J. Pyne, Fire: a Brief History, University of Washington Press, 2019. https://books.google.com.hk/books?hl=zh-CN&lr=&id=kKakDwAAQBAJ&oi=fnd&pg.
[3] Y. Zong, Z. Chen, J.B. Innes, C. Chen, Z. Wang, H. Wang, Fire and flood management of coastal swamp enabled first rice paddy cultivation in east China, Nature 449 (2007) 459–462. https://doi-org.3267.top/10.1038/nature06135.
[4] X. Wang, J. Xiao, L. Cui, Z. Ding, Holocene changes in fire frequency in the Daihai Lake region (north-central China): indications and implications for an important role of human activity, Quat. Sci. Rev. 59 (2013) 18–29, https://doi.org/10.1016/j.quascirev.2012.10.033.
[5] J.R. Marlon, P.J. Bartlein, A. Daniau, S.P. Harrison, S.Y. Maezumi, M.J. Power, W. Tinner, B. Vanniére, Global biomass burning: a synthesis and review of Holocene paleofire records and their controls, Quat. Sci. Rev. 65 (2013) 5–25. https://doi-org-ssl.8611.top/10.1016/j.quascirev.2012.11.029.
[6] W. Pei, S. Wan, P.D. Clift, J. Dong, X. Liu, J. Lu, Y. Tan, X. Shi, A. Li, Human impact overwhelms long-term climate control of fire in the Yangtze River Basin since 3.0 ka BP, Quat. Sci. Rev. 230 (2020), 106165, https://doi.org/10.1016/j.quascirev.2020.106165.
[7] M.C.L. Forget, L. Regev, D.E. Friesemc, R. Shahack-Gross, Physical and mineralogical properties of experimentally heated chaff-tempered mud bricks: implications for reconstruction of environmental factors influencing the appearance of mud bricks in archaeological conflagration events, J. Archaeol. Sci. Rep. 2 (2015) 80–93, https://doi.org/10.1016/j.jasrep.2015.01.008.
[8] E.M. Pérez-Monserrat, M. Causarano, L. Maritan, A. Chavarria, G.P. Brogiolo, G. Cultrone, Roman brick production technologies in padua (northern Italy) along the late antiquity and medieval times: durable bricks on high humid environs, J. Cult. Herit. 54 (2022) 12–20, https://doi.org/10.1016/j.culher.2022.01.007.
[9] J. Liu, Z. Zhang, Characteristics and weathering mechanisms of the traditional Chinese blue brick from the ancient city of Ping Yao, R. Soc. Open Sci. 7 (2020), 200058, https://doi.org/10.1098/rsos.200058.
[10] A.K. Mishra, A. Mishra, Anshumali, Geochemical characterization of bricks used in historical monuments of 14-18th century CE of Haryana region of the Indian subcontinent: reference to raw materials and production technique, Construct. Build. Mater. 269 (2021), 121802, https://doi.org/10.1016/j.conbuildmat.2020.121802.
[11] J. Zhu, Y. Zhang, T. Wang, C.H. Zhao, J.C. Yu, M.D. Glascock, C.S. Wang, Determining the firing temperature of low-fired ancient pottery: an example from the donghulin site, Beijing, China, Archaeometry 56 (2014) 562–572, https://doi.org/10.1111/arcm.12033.
[12] B. Yan, S. Liu, M.L. Chastain, S. Yang, J. Chen, A new FTIR method for estimating the firing temperature of ceramic bronze-casting moulds from early China, Sci. Rep. 11 (2021) 3316, https://doi.org/10.1038/s41598-021-82806-z.
[13] R. De Luca, V. Gigliotti, M. Panarello, A. Bloise, G.M. Crisci, D. Miriello, Spectroscopic, microchemical and petrographic analyses of plasters from ancient buildings in Lamezia Terme (Calabria, Southern Italy), Spectrochim, Acta. A. Mol. Biomol. Spectrosc. 153 (2016) 184–193, https://doi.org/10.1016/j.saa.2015.08.018.
[14] N. Jordanova, D. Jordanova, M. Kostadinova-Avramova, D. Lesigyarski, V. Nikolov, G. Katsarov, K. Bacvarov, A mineral magnetic approach to determine paleo-firing temperatures in the neolithic settlement site of mursalevo-deveboaz (SW Bulgaria), J. Geophys. Res. Solid Earth 123 (2018) 2522–2538, https://doi.org/10.1002/2017JB015190.
[15] F. Clegg, C. Breen, M.A. Carter, C. Ince, S.D. Savage, M.A. Wilson, Dehydroxylation and rehydroxylation mechanisms in fired clay ceramics: a TG–MS and DRIFTS investigation, J. Am. Ceram. Soc. 95 (2012) 416–422, https://doi.org/10.1111/j.1551-2916.2011.04926.x.
[16] R. Thompson, F. Oldfield, Environmental Magnetism, Allen and Unwin, Winchester, Mass (1986), https://doi.org/10.1007/978-94-011-8036-8.
[17] M. Evans, F. Heller, Environmental Magnetism: Principles and Applications of Enviromagnetics, Elsevier, 2003. https://books.google.com.hk/books?hl=zh-CN&lr=&id=fU5orRv4qxYC&oi=fnd&pg.
[18] Q. Liu, A.P. Roberts, J.C. Larrasoaña, S.K. Banerjee, Y. Guyodo, L. Tauxe, F. Oldfield, Environmental magnetism: principles and applications, Rev. Geophys. 50 (2012) 1–50, https://doi.org/10.1029/2012RG000393.
[19] K.L. Rasmussen, G.A. De La Fuente, A.D. Bond, K.K. Mathiesen, S.D. Vera, Pottery firing temperatures: a new method for determining the firing temperature of ceramics and burnt clay, J. Archaeol. Sci. 39 (2012) 1705–1716, https://doi.org/10.1016/j.jas.2012.01.008.
[20] E. Tema, E. Ferrara, Magnetic measurements as indicator of the equivalent firing temperature of ancient baked clays: new results, limits and cautions, J. Cult. Herit. 35 (2019) 64–75, https://doi.org/10.1016/j.culher.2018.05.008.
[21] N. Jordanova, D. Jordanova, V. Barrón, D. Lesigyarski, M. Kostadinova-Avramova, Rock-magnetic and color characteristics of archaeological samples from burnt clay from destructions and ceramics in relation to their firing temperature, Archaeol. Anthropol. Sci. 11 (2019) 3595–3612, https://doi.org/10.1007/s12520-019-00782-y.
[22] X. Li, Y. Wu, L. Mao, X. Wu, Y. Song, Determination of the thermal temperatures of burnt clay at Sujiacun site based on magnetic susceptibility, Science of conservation and archaeology 34 (2022) 63–70, https://doi.org/10.16334/j.cnki.cn31-1652/k.20200901886. In Chinese with English abstract.
[23] N. Linford, E. Platzman, Estimating the approximate firing temperature of burnt archaeological sediments through an unmixing algorithm applied to hysteresis data, Phys. Earth Planet. In. 147 (2004) 197–207, https://doi.org/10.1016/j.pepi.2004.06.007.
[24] S. Spassov, J. Hus, Estimating baking temperatures in a Roman pottery kiln by rock magnetic properties: implications of thermochemical alteration on archaeointensity determinations, Geophys. J. Int. 167 (2006) 592–604, https://doi.org/10.1111/j.1365-246X.2006.03114.x.
[25] J. López-Sánchez, A. Palencia-Ortas, A. del Campo, G. McIntosh, M. Kovacheva, F. Martín-Hernández, N. Carmona, O. Rodríguez de la Fuente, P. Marín, A. Molina-Cardín, M.L. Osete, Further progress in the study of epsilon iron oxide in archaeological baked clays, Phys. Earth Planet. In. 307 (2020), 106554, https://doi.org/10.1016/j.pepi.2020.106554.
[26] N. Jordanova, D. Jordanova, D. Lesigyarski, M. Kostadinova-Avramova, Imprints of paleo-environmental conditions and human activities in mineral magnetic properties of fired clay remains from Neolithic houses, J. Archaeol. Sci. Rep. 33 (2020), 102473, https://doi.org/10.1016/j.jasrep.2020.102473.
[27] P. Dolukhanov, A. Shukurov, D. Gronenborn, D. Sokoloff, V. Timofeev, G. Zaitseva, The chronology of neolithic dispersal in central and eastern Europe, J. Archaeol. Sci. 32 (2005) 1441–1458. https://doi-org-ssl.8611.top/10.1016/j.jas.2005.03.021.
[28] A.P. Underhill (Ed.), A Companion to Chinese archaeology , John, Wiley & Sons, 2013. https://books.google.com.hk/books?hl=zhCN&lr=&id=I3XG3H_WlM8C&oi=fnd&pg.
[29] H. Xu, Erlitou: the origin of the tradition of non-fortified primary capitals in early China, Archaeol. Res. Asia 14 (2018) 71–79, https://doi.org/10.1016/j.ara.2017.11.003.
[30] O. García-Puchol, D.C. Salazar-García (Eds.), Times of Neolithic Transition along the Western Mediterranean, Springer International Publishing, Cham, 2017, https://doi.org/10.1007/978-3-319-52939-4.
[31] X. Wu, C. Zhang, P. Goldberg, D. Cohen, Y. Pan, T. Arpin, O. Bar-Yosef, Early pottery at 20,000 years ago in Xianrendong Cave, China, Science 336 (2012) 1696–1700, https://doi.org/10.1126/science.1218643.
[32] D.J. Cohen, The Neolithic of southern China, in: C. Renfrew, P. Bahn (Eds.), The Cambridge World Prehistory, East Asia and the Americas – Part V: 5, 2, Cambridge University Press, New York, 2014, pp. 765–781, https://doi.org/10.1017/CHO9781139017831.053.
[33] D. Hosner, M. Wagner, P.E. Tarasov, X. Chen, C. Leipe, Spatiotemporal distribution patterns of archaeological sites in China during the Neolithic and Bronze Age: an overview, Holocene 26 (2016) 1576–1593, https://doi.org/10.1177/0959683616641743.
[34] C. Zhang, A.M. Pollard, J. Rawson, L. Huan, R. Liu, X. Tang, China's major Late Neolithic centres and the rise of Erlitou, Antiquity 93 (2019) 588–603, https://doi.org/10.15184/aqy.2019.63.
[35] R.M. Arbogast, S. Jacomet, M. Magny, J. Schibler, The significance of climate fluctuations for lake level changes and shifts in subsistence economy during the late Neolithic (4300–2400 B.C.) in central Europe, Veg. Hist. Archaeobotany 15 (2006) 403–418, https://doi.org/10.1007/s00334-006-0053-y.
[36] T. Fernández-Crespo, C. Snoeck, J. Ordoño, N.J. De Winter, A. Czermak, N. Mattielli, J.A. Lee-Thorp, R.J. Schulting, Multi-isotope evidence for the emergence of cultural alterity in Late Neolithic Europe, Sci. Adv. 6 (2020), eaay2169, https://doi.org/10.1126/sciadv.aay2169.

[37] J. Jin, F. Li, Z. Ling, Z. Li, New chronological evidence reveals a continuously inhabited Neolithic–historical settlement in south China, Palaeogeogr. Palaeoclimatol. Palaeoecol. 600 (2022), 111081. https://doi-org-ssl.8611.top/10.1016/j.palaeo.2022.111081.

[38] L. Zhao, C. Ma, C. Leipe, T. Long, K. Liu, H. Lu, L. Tang, Y. Zhang, M. Wagner, P.E. Tarasov, Holocene vegetation dynamics in response to climate change and human activities derived from pollen and charcoal records from southeastern China, Palaeogeogr. Palaeoclimatol. Palaeoecol. 485 (2017) 644–660, https://doi.org/10.1016/j.palaeo.2017.06.035.

[39] J. Jin, X. Cai, Y. Huang, X. Zuo, Z. Ling, J. Dai, Y. Ren, W. Zhang, S. Li, New luminescence dating evidence reveals the timing of Neolithic human activities in Fuzhou Basin, South China, Catena 207 (2021), 105590, https://doi.org/10.1016/j.catena.2021.105590.

[40] P.P. Kruiver, M.J. Dekkers, D. Heslop, Quantification of magnetic coercivity components by the analysis of acquisition curves of isothermal remanent magnetization, Earth Planet Sci. Lett. 189 (2001) 269–276, https://doi.org/10.1016/S0012-821X(01)00367-3.

[41] A.P. Roberts, C.R. Pike, K.L. Verosub, First-order reversal curve diagrams: a new tool for characterizing the magnetic properties of natural samples, J. Geophys. Res. Solid Earth 105 (28) (2000), https://doi.org/10.1029/2000jb900326, 461-28,475.

[42] S. Deng, P. Fan, Y. Tang, L. Tan, Z. Wang, L. Huang, H. Xu, Determination of 9 kinds of soil pollution of heavy metals elements in samples by X-ray fluorescence spectrometry, Chin. J. Inorg. Chem. 9 (2019) 12–15, https://doi.org/10.3969/j.issn.2095-1035.2019.04.003.

[43] P.J. Reimer, E. Bard, A. Bayliss, J.W. Beck, P.G. Blackwell, C. Bronk Ramsey, C.E. Buck, R.L. Edwards, M. Friedrich, P.M. Grootes, T.P. Guilderson, H. Haflidason, I. Hajdas, C. Hatté, T.J. Heaton, D.L. Hoffmann, A.G. Hogg, K.A. Hughen, K.F. Kaiser, B. Kromer, S.W. Manning, M. Niu, R.W. Reimer, D. A. Richards, M.E. Scott, J.R. Southon, C.S.M. Turney, J. van der Plicht, IntCal13 and Marine13 radiocarbon age calibration curves 0-50,000 yr cal BP, Radiocarbon 55 (2013) 1869–1887, https://doi.org/10.2458/azu_js_rc.55.16947.

[44] I. Johari, S. Said, B. Hisham, A. Bakar, Z.A. Ahmad, Effect of the change of firing temperature on microstructure and physical properties of clay bricks from beruas (Malaysia), Sci. Sinter. 42 (2010) 245–254, https://doi.org/10.2298/SOS1002245J.

[45] Y. Tong, C. Wang, Application and exploration of the thermal expansion technology in determination of the firing temperature of ancient ceramics, Natural Science Edition 23 (2017) 33–34, https://doi.org/10.16177/j.cnki.gxmzzk.2017.03.006. In Chinese with English abstract.

[46] J. Jin, Z. Li, X. Chen, X. Jiang, S. Qi, M. Wu, S. Zhu, F. Chen, G. Ye, The geochemical records and their paleoclimate significance of the red weathering crust at Changle coast in central Fujian since 1.2Ma, Journal of Huazhong Normal University (Natural Science) 46 (2012) 780–788, https://doi.org/10.19603/j.cnki.1000-1190.2012.06.028. In Chinese with English abstract.

[47] S. Qi, The Study of Cause and Sedimentary Environment of Quanternary Red Earth in Fujian, Fujian Normal University, 2012. In Chinese with English abstract, Master Thesis.

[48] Q. Zhang, E. Appel, Reversible thermal hysteresis in heating-cooling cycles of magnetic susceptibility: a fine particle effect of magnetite, Geophys. Res. Lett. 50 (2023), https://doi.org/10.1029/2023GL102932 e2023GL102932.

[49] A.R. Muxworthy, D.J. Dunlop, First-order reversal curve (FORC) diagrams for pseudo-single-domain magnetites at high temperature, Earth, Planet. Sci. Lett. 203 (2002) 369–382, https://doi.org/10.1016/S0012-821X(02)00880-4.

[50] R. Day, M. Fuller, V.A. Schmidt, Hysteresis properties of Titanomagnetites: grain size and compositional dependence, Phys. Earth Planet. In. 13 (1977) 260–267, https://doi.org/10.1016/0031-9201(77)90108-X.

[51] D.J. Dunlop, Theory and application of the Day plot (Mrs/Ms versus Hcr/Hc)1. Theoretical curves and test using titanomagnetite data, J. Geophys. Res. 107 (2002) 2056, https://doi.org/10.1029/2001JB000486.

[52] Q. Liu, C. Deng, Y. Yu, J. Torrent, M.J. Jackson, S.K. Banerjee, R. Zhu, Temperature dependence of magnetic susceptibility in an argon environment: implications for pedogenesis of Chinese loess/palaeosols, Geophys. J. Int. 161 (2005) 102–112, https://doi.org/10.1111/j.1365-246X.2005.02564.x.

[53] J.A. Dearing, R.J.L. Dann, K. Hay, J.A. Lees, P.J. Loveland, B.A. Maher, K. O'Grady, Frequency-dependent susceptibility measurements of environmental materials Frequency-dependent susceptibility measurements of environmental materials, Geophys. J. Int. 124 (1996) 228–240, https://doi.org/10.1111/j.1365-246X.1996.tb06366.x.

[54] J. Chapmann, Deliberate house-burning in the prehistory of central and eastern Europe, in: Glyferocharkeologiskarum: Envänbok till Jarl Nordbladh, University of Göteborg Press, Durham, UK, 1999. http://dro.dur.ac.uk.

[55] N. Li, Preliminary study on building foundation of Lingjiatan braised soil relic, Scientific research on Chinese cultural relics 3 (2008) 63–66. In Chinese with English abstract, https://kns-cnki-net-s.z.library.sh.cn/kcms2/article/abstract?v.

[56] R.V. Bellomo, A methodological approach for identifying archaeological evidence of fire resulting from human activities, J. Archaeol. Sci. 20 (1993) 525–553, https://doi.org/10.1006/jasc.1993.1033.

[57] R. Jones, The decoration and firing of ancient Greek pottery: a review of recent investigations, Advances in Archaeomaterials 2 (2021) 67–127, https://doi.org/10.1016/j.aia.2021.07.002.

[58] I.J. Glasspool, A.C. Scott, D. Waltham, N. Pronina, L. Shao, The impact of fire on the Late Paleozoic Earth system, Front. Plant Sci. 6 (2015) 756, https://doi.org/10.3389/fpls.2015.00756.

[59] M. Ivanova, B. De Cupere, J. Ethier, E. Marinova, Pioneer farming in southeast Europe during the early sixth millennium BC: climate-related adaptations in the exploitation of plants and animals, PLOS, ONE 13 (2018), e0197225, https://doi.org/10.1371/journal.pone.0202668.

[60] M. Dubale, M.V. Vasic, G. Goel, A. Kalamdhad, L.B. Singh, Utilization of construction and demolition mix waste in the fired brick production: the impact on mechanical properties, Materials 16 (2023), https://doi.org/10.3390/ma16010262.

[61] C. Beatrice, M. Coïsson, E. Ferrara, E.S. Olivetti, Relevance of magnetic properties for the characterization of burnt clays and archaeological tiles, Phys. Chem. Earth, Parts A/B/C 33 (2008) 458–464, https://doi.org/10.1016/j.pce.2008.02.018.

[62] B.A. Maher, Palaeoclimatic records of the loess/palaeosol sequences of the Chinese Loess Plateau, Quat. Sci. Rev. 154 (2016) 23–84, https://doi.org/10.1016/j.quascirev.2016.08.004.

[63] S. Lu, Lithological factors affecting magnetic susceptibility of subtropical soils, Zhejiang Province, China, Catena 40 (2000) 359–373, https://doi.org/10.1016/S0341-8162(00)00092-8.

[64] T.P. Almeida, A. Muxworthy, W. William, R.E. Dunin-Borkowski, Oxidation of peseudo-single domain Fe_3O_4 particles and associated magnetic response examined by environmental TEM and off-Axis electron holography, Microsc. Microanal. 19 (2013) 1456–1457, https://doi.org/10.1017/S1431927613009276.

[65] J. Torrent, Q. Liu, J. Bloemendal, V. Barrón, Magnetic enhancement and iron oxides in the upper Luochuan loess–paleosol sequence, Chinese Loess Plateau, Soil Sci. Soc. Am. J. 71 (2007) 1570–1578, https://doi.org/10.2136/sssaj2006.0328.

[66] X. Liu, Recent and Holocene Stratigraphy of the Diaokou Lobe Area in the Huanghe Delta Based on Grain Size and Magnetic Properties, Ocean University of China, 2013, https://doi.org/10.14027/j.cnki.cjxb.2014.03.015. In Chinese with English abstract.

[67] G. Jia, Sedimentary Characteristics and Environmental Significance of Loess of the BZ Core, on Daheishan Island, Shandong Province, Shandong Normal University, 2017, https://doi.org/10.11928/j.issn.1001-7410.2017.03.09. In Chinese with English abstract.

[68] C. Liu, C. Deng, Q. Liu, Mineral magnetic studies of the vermiculated red soils in southeast China and their paleoclimatic significance, Palaeogeogr. Palaeoclimatol. Palaeoecol. 329–330 (2012) 173–183, https://doi.org/10.1016/j.palaeo.2012.02.035.

[69] W. Zhang, C. Dong, L. Ye, H. Ma, L. Yu, Magnetic properties of coastal loess on the Midao islands, northern China: implications for provenance and weathering intensity, Palaeogeogr. Palaeoclimatol. Palaeoecol. 333–334 (2012) 160–167, https://doi.org/10.1016/j.palaeo.2012.03.026.

[70] T. Brücher, V. Brovkin, S. Kloster, J.R. Marlon, M.J. Power, Comparing modelled fire dynamics with charcoal records for the Holocene, Clim. Past 10 (2014) 811–824, https://doi.org/10.5194/cp-10-811-2014.

[71] D.L. Thatcher, A.D. Wanamaker, R.F. Denniston, Y. Asmerom, V.J. Polyak, D. Fullick, C.C. Ummenhofer, D.P. Gillikin, J.A. Haws, Hydroclimate variability from western Iberia (Portugal) during the Holocene: insights from a composite stalagmite isotope record, Holocene 30 (2020) 966–981, https://doi.org/10.1177/0959683620908648.

[72] J. Dabkowski, J. Frodlová, M. Hájek, P. Hájková, L. Petr, D. Fiorillo, L. Dudová, M. Horsák, A complete Holocene climate and environment record for the Western Carpathians (Slovakia) derived from a tufa deposit, Holocene 29 (2019) 493–504, https://doi.org/10.1177/0959683618816443.

[73] S. Tonkov, Holocene palaeovegetation of the Northwestern Pirin Mountains (Bulgaria) as reconstructed from pollen analysis, Rev. Palaeobot. Palynol. 124 (2003) 51–61, https://doi.org/10.1016/S0034-6667(02)00247-6.
[74] W. Finsinger, D. Colombaroli, J. De Beaulieu, V. Valsecchi, B. Vannière, E. Vescovi, E. Chapron, A.F. Lotter, M. Magny, W. Tinner, Early to mid-Holocene climate change at Lago dell'Accesa (central Italy): climate signal or anthropogenic bias? J. Quat. Sci. 25 (2010) 1239–1247, https://doi.org/10.1002/jqs.1402.
[75] Q. Wang, Thermal Temperature Study of Earth Burning Materials in Prehistoric Building, Nanjing University of Information Science & Technology, 2022. In Chinese with English abstract, Ph.D Thesis.
[76] Y. Wang, H. Cheng, R.L. Edwards, Y. He, X. Kong, Z. An, J. Wu, M.J. Kelly, C.A. Dykoski, X. Li, The Holocene asian monsoon: links to solar changes and north atlantic climate, Science 308 (2005) 854–857, https://doi.org/10.1126/science.1106296.
[77] K. Yu, Coral reefs in the South China Sea: their response to and records on past environmental changes, Sci. China Earth Sci. 55 (2012) 1217–1229, https://doi.org/10.1007/s11430-012-4449-5.
[78] J. Li, J. Dodson, H. Yan, W. Wang, J.B. Innes, Y. Zong, X. Zhang, Q. Xu, J. Ni, F. Lu, Quantitative Holocene climatic reconstructions for the lower Yangtze region of China, Clim. Dynam. 50 (2018) 1101–1113, https://doi.org/10.1007/s00382-017-3664-3.
[79] B. Song, S. Yi, S. Yu, W. Nahm, J. Lee, J. Lim, J. Kim, Z. Yang, M. Han, K. Jo, Y. Saito, Holocene relative sea-level changes inferred from multiple proxies on the west coast of South Korea, Palaeogeogr. Palaeoclimatol. Palaeoecol. 496 (2018) 268–281, https://doi.org/10.1016/j.palaeo.2018.01.044.
[80] North Greenland Ice Core Project members, High-resolution record of Northern Hemisphere climate extending into the last interglacial period, Nature 431 (2004) 147–151, https://doi.org/10.1038/nature02805.
[81] G. Bond, B. Kromer, J. Beer, R. Muscheler, M.N. Evans, W. Showers, S. Hoffmann, R. Lotti-Bond, I. Hajdas, G. Bonani, Persistent solar influence on north atlantic climate during the Holocene, Science 294 (2001) 2130–2136, https://doi.org/10.1126/science.1065680.
[82] A.I. Bartlett, R.M. Hadden, L.A. Bisby, A review of factors affecting the burning behaviour of wood for application to tall timber construction, Fire Technol. 55 (2018) 1–49, https://doi.org/10.1007/s10694-018-0787-y.
[83] E. Githumbi, R. Fyfe, M.J. Gaillard, A.K. Trondman, F. Mazier, A.B. Nielsen, A. Poska, S. Sugita, J. Woodbridge, J. Azuara, A. Feurdean, R. Grindean, V. Lebreton, L. Marquer, N. Nebout-Combourieu, M. Stančikaitė, I. Tanţău, S. Tonkov, L. Shumilovskikh, LandClimII data contributors, European pollen-based REVEALS land-cover reconstructions for the Holocene: methodology, mapping and potentials, Earth Syst. Sci. Data 14 (2022) 1581–1619, https://doi.org/10.5194/essd-14-1581-2022.
[84] H. Niu, L. Marquer, D. Sack, G. Gao, J. Wang, M. Meng, D. Jie, Middle to late Holocene plant cover variation in relation to climate, fire and human activity in the Songnen grasslands of northeastern China, Front. Plant Sci. 13 (2023), 1071273, https://doi.org/10.3389/fpls.2022.1071273.
[85] Y. Guo, D. Mo, L. Mao, S. Wang, S. Li, Settlement distribution and its relationship with environmental changes from the neolithic to Shang-Zhou dynasties in northern Shandong, China, J. Geogr. Sci. 23 (2013) 679–694, https://doi.org/10.1007/s11442-013-1037-3.
[86] L. Liu, X. Chen, H. Wright, H. Xu, Y. Li, G. Chen, H. Zhao, H. Kim, G. Lee, Rise and fall of complex societies in the Yiluo region, North China: the spatial and temporal changes, Quat. Int. 521 (2019) 4–15, https://doi.org/10.1016/j.quaint.2019.05.025.
[87] D.S. Kaufman, E. Broadman, Revisiting the Holocene global temperature conundrum, Nature 614 (2023) 425–435, https://doi.org/10.1038/s41586-022-05536-w.